

## $H_\infty$ controller design for a 4-meter direct-drive azimuth axis

Li-Yan Chen<sup>1,2,3</sup>, Zhen-Chao Zhang<sup>1,2</sup>, Xiao-Li Song<sup>1,2</sup> and Da-Xing Wang<sup>1,2</sup>

<sup>1</sup> National Astronomical Observatories / Nanjing Institute of Astronomical Optics & Technology, Chinese Academy of Sciences, Nanjing 210042, China; *lychen@niaot.ac.cn*

<sup>2</sup> Key Laboratory of Astronomical Optics & Technology, Nanjing Institute of Astronomical Optics & Technology, Chinese Academy of Sciences, Nanjing 210042, China

<sup>3</sup> University of Chinese Academy of Sciences, Beijing 100049, China

Received 2014 November 3; accepted 2015 May 5

**Abstract** To pursue a higher imaging resolution for exploring more details in the information conveyed by the Universe, the next generation of optical telescopes based on a direct drive widely employ the extremely large aperture structure, which also introduces more disturbances and uncertain factors to the control system. Facing this new challenge, the PID control method in main-axis control systems of traditional astronomical telescopes cannot suffice for the requirement of the tracking precision and disturbance sensitivity in angular velocity. To overcome this shortcoming, we establish a dynamic model and propose an  $H_\infty$  controller for a 4-meter azimuth direct drive control system that consists of a revolving platform (azimuth axis), a three-phase torque motor, a motor drive, an encoder, a data acquisition card and a small computers. Simulations are carried out to analyze the model and guide the real experiments. Experimental results show that the proposed  $H_\infty$  controller reduces the tracking error by a maximum of 80.69% (average 57.8%) and the disturbance sensitivity by a maximum of 82.3% (average 50.96%) compared with the traditional tuned PI controller; furthermore, the order of the model describing the proposed controller can be reduced to three, thus its feasibility in real systems is guaranteed.

**Key words:**  $H_\infty$  control — direct-drive telescope — PMSM — disturbance rejection

### 1 INTRODUCTION

The extremely large aperture structure (ELAS) design is widely applied to new generation ground-based direct-drive astronomical telescopes, such as the Very Large Telescope (VLT) and the Gran Telescopio Canarias (GTC), to acquire more information about the Universe. On one hand, the ELAS can achieve a higher imaging resolution, which is a desired significant characteristic in the design of telescopes; however, on the other hand, the large aperture structure concomitantly introduces extra negative influences to many aspects, e.g. wind shakes, the thermal effect (Erm & Gutierrez 2000; Cho et al. 2001; Angeli et al. 2002; Farahani et al. 2012), and unexpected disturbance (Antoniou et al. 1992; Carlstrom et al. 2011). These disadvantages present a challenge to the required stability of the control system, especially for the direct-drive scheme.

For control systems of the main axes of telescopes applied in the field of astronomy, the PID controller is widely adopted for the control of angular velocity because of its simplicity. The VLT

utilizes a typical PI controller with the feed-forward method and a certain number of filters; the GTC selects a dual-feedback PI controller with excess filters; the Thirty Meter Telescope (TMT) plans to implement PID feedback. Nonetheless, the disadvantages inherent in the ELAS design make PID controllers unable to stabilize angular velocity; so it is difficult for the VLT to resist wind disturbances (Ravensbergen 1994); the GTC is ineffective in controlling the disturbance caused by extremely flukey changes in wind and other uncertain sources that suddenly appear (Suárez et al. 2008). Thus, advanced control methods should be considered in the future design of the controller used on astronomical telescopes to satisfy the requirements of both high accuracy and excellent performance in disturbance rejection.

$H_\infty$  control theory has attracted much attention during the past decades because of the robust characteristics provided by its controllers (Ortega & Rubio 2004). As a controller that focuses on the minimization problem in maximal energy-limited disturbance suppression within the working frequency band and guarantees performance in a worst-case scenario (Kwakernaak 1993), the  $H_\infty$  method is an ideal candidate for handling uncertain disturbances in large aperture telescopes. So far, although the  $H_\infty$  control method has been applied to the field of astronomy, the current situation remains immature. For example, studies of its applications in the control systems for main axes of antennae that are part of radio telescopes (Gawronski 2001) and in segmented mirrors that are part of the TMT (Baris Ulutas & Jennifer Dunn 2012) have only been simulations.

To solve the disturbance rejection and stabilization problems in the control systems for the main axes and to achieve a better steady-state performance that is more significant for large telescopes, we propose an  $H_\infty$  controller for the 4-meter azimuth direct-drive control system, and establish a dynamic model via least-squares (LS) estimation. To evaluate the performance of the proposed controller, a comparison of the steady-state response errors between the traditional PI controller and the proposed controller for system inputs contaminated by different types of disturbance and frequencies is carried out by simulation. The two controllers are also tested on a real closed-loop control system. The quantified comparison results for tracking error and disturbance sensitivity are given.

Section 2 introduces our experiment environment, establishes the mathematical model for the 4-meter direct-drive motor, and identifies the parameters of the model. Section 3 designs an  $H_\infty$  controller for the motor. Section 4 states the simulation results of the  $H_\infty$  controller for inputs with disturbances. Section 5 shows the implementation of the  $H_\infty$  controller, and compares its performance with PID controllers via experiments. Finally, Section 6 concludes.

## 2 SYSTEM MODEL AND IDENTIFICATION

### 2.1 System Structure

The 4-meter azimuth direct-drive control system consists of an azimuth axis, a three-phase torque motor, a motor drive, a photoelectric encoder, a small computer and a data acquisition card. The revolving platform has a diameter of 3.76 meters and a weight of 11.2 tons, as shown in Figure 1(a). The rotary direct-drive motor (with a peak torque of 2313 N·m in the linear range; 3145 N·m in the saturation range) is installed coaxially under the platform. The photoelectric encoder is installed on the stator. A metronix<sup>TM</sup> motor drive ARS 2310 FS is used to control the motor, as shown in Figure 1(b). Before the motor starts to work, the rotor will be floated by the hydraulic system. The small computer connects the motor drive through the serial port, receiving the parameters of the motor and sending control instructions. The velocity of the rotor is sampled by the PCI-1784U data acquisition card which acquires pulse signals from the encoder. The  $H_\infty$  controller is implemented via the small computer.

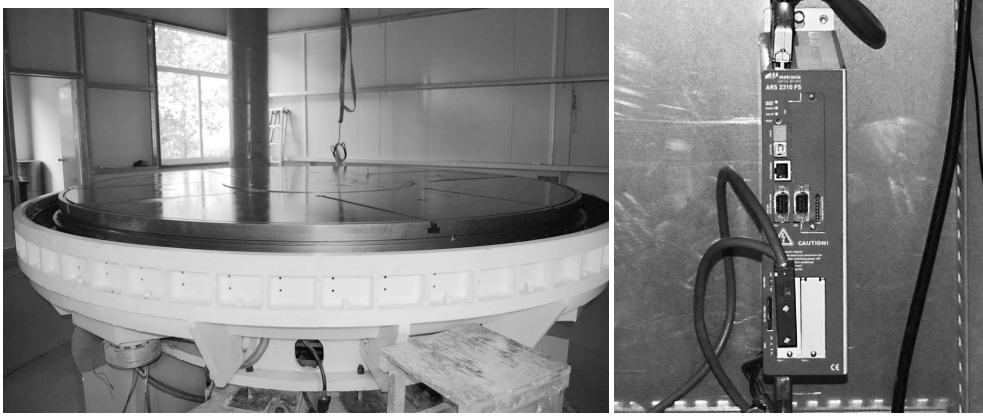


**Fig. 1** System structure: (a) 3.76-meter revolving platform. (b) metronix™ motor drive ARS 2310 FS. The three-phase permanent magnet synchronous motor, with a direct drive that is powered by the motor drive, can provide a peak torque of 2313 N·m in the linear range and 3145 N·m in the saturation range. The motor and the revolving platform are coaxial.

## 2.2 Model and Identification

The behavior of the three-phase permanent magnet synchronous motor can be expressed in the model in the rotor reference frame as

$$\frac{d}{dt}i_d = \frac{1}{L_d}v_d - \frac{R}{L_d}i_d + \frac{L_q}{L_d}p\omega_r i_q, \quad (1)$$

$$\frac{d}{dt}i_q = \frac{1}{L_q}v_q - \frac{R}{L_q}i_q - \frac{L_d}{L_q}p\omega_r i_d - \frac{\lambda p\omega_r}{L_q}, \quad (2)$$

$$T_e = \frac{3}{2}p \left[ \lambda i_q + (L_d - L_q) i_d i_q \right], \quad (3)$$

where  $L_q$  and  $L_d$  respectively denote the quadrature-axis (q-axis) and the direct-axis (d-axis) inductances;  $R$  denotes the resistance of the stator windings;  $i_q$  and  $i_d$  denote the q-axis and d-axis currents respectively;  $v_q$  and  $v_d$  denote the q-axis and d-axis voltages respectively;  $\omega_r$  denotes the angular velocity of the rotor;  $\lambda$  denotes the amplitude of the flux induced by the permanent magnets of the rotor in the stator phases;  $p$  denotes the number of pole pairs;  $T_e$  denotes the electromagnetic torque (Krause et al. 2013). To simplify the implementation, the reference of  $i_d$  is set to zero in the current control loop (Louis 2013), so the electromagnetic torque is proportional to  $i_q$  as

$$T_e(t) = k_m i_q(t), \quad (4)$$

where  $k_m$  is a constant. For large telescopes directly driven by motors, the rate of change for the current is much faster than that of the angular speed of the platform (the typical value is only 360° per 24 hours), thus for the current control loop, the counter-electromotive force (counter EMF) can be considered to be invariant during the time that the current transition occurs (Dixon et al. 1996). By ignoring the counter EMF effect and the d-axis current  $i_d$ , the current control loop can be described by a simple model like that of a DC motor, as shown in Figure 2. The closed-loop current control transfer function can be obtained from Figure 2(c)

$$G_c(s) = \frac{I_q(s)}{I_q^*(s)} = \frac{I_q(s)}{U_q^*(s)/\beta} = \frac{K_I}{T_{\Sigma i} s^2 + s + K_I}, \quad (5)$$

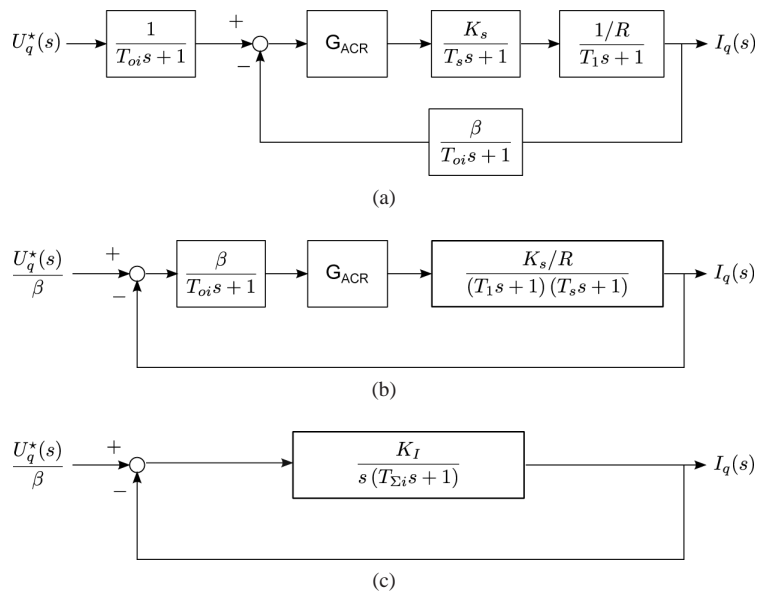


**Fig. 2** Classic simplification of the q-axis current control loop (Ruan & Chen 2006).  $U_q^*(s)$  denotes the reference voltage for a desired current  $I_q(s)$ ,  $G_{ACR}$  denotes the transfer function of the automatic current regulator (ACR),  $\beta$  and  $T_{oi}$  respectively denote the amplification factor and the time constant of the current feedback filter,  $K_s$  and  $T_s$  respectively denote the amplification factor and the time constant of the thyristor trigger and rectifier module, and  $R$  and  $T_1$  respectively denote the resistance and the time constant of the armature. (a) The original model ignoring the counter EMF effect. (b) The equivalent block diagram with a unit negative feedback. (c) Simplification. Designed as a PI controller,  $G_{ACR} = K_i \frac{(T_1 s + 1)}{T_1 s}$  where  $K_i$  is the proportional term, and the ACR eliminates  $T_1 s + 1$  in the denominator to regulate the open-loop transfer function as  $G_o(s) = \frac{K_I}{s(T_{oi} s + 1)(T_s s + 1)}$  where  $K_I = \frac{K_s K_s \beta}{T_1 R}$ ; then because  $T_{oi}$  and  $T_s$  are small, the term  $\frac{1}{(T_{oi} s + 1)(T_s s + 1)}$  is further simplified as  $\frac{1}{T_{\Sigma i} s + 1}$ , where  $T_{\Sigma i} = T_{oi} + T_s$ .

where  $K_I$  is a constant coefficient properly regulated by the automatic current regulator (ACR), and  $T_{\Sigma i}$  is used for merging the effects of the poles caused by the *current feedback filter* and the *thyristor trigger and rectifier module*. The angular velocity open-loop control adopts the classic mechanical model  $T_L(t) = J\dot{\omega}(t) + \mu\omega(t)$ , where  $T_L$  is the load torque,  $J$  is the moment of inertia of the revolving platform,  $\mu$  is the coefficient of friction, and  $\omega(t)$  is the angular velocity (Dorf & Bishop 2011). When ignoring the disturbance torque (actually it is considered to be the disturbance to the input reference current in the next section),  $T_e(t) = T_L(t)$ , thus the transfer function from the q-axis current to the angular velocity is

$$G_v(s) = \frac{\Omega(s)}{I_q(s)} = \frac{k_m}{Js + \mu} \tag{6}$$

Consider the angular velocity open-loop transfer function

$$G(s) = G_c(s)G_v(s) = \frac{k_m/\mu}{\left[ \left( \sqrt{\frac{T_{\Sigma i}}{K_I}} s \right)^2 + \frac{1}{K_I} s + 1 \right] \left( \frac{J}{\mu} s + 1 \right)}, \tag{7}$$

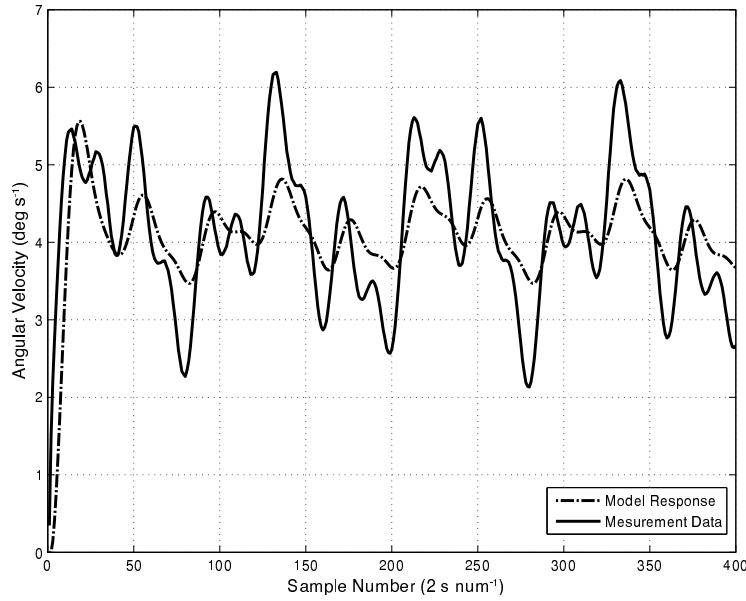


**Fig. 3** Comparison of the responses between the model and the measured data to the mixed sinusoidal input  $i_q^*(t) = 8 + 0.5 \sin(2\pi \cdot 0.1t) + 0.5 \sin(2\pi \cdot 0.05t) + 0.5 \sin(2\pi \cdot 0.02t)$  A,  $0 \leq t \leq 800$  s. The sampling period is 2 s. The root-mean-square error is  $0.7095 \text{ deg s}^{-1}$  in this trial.

in which generally  $T_{\Sigma i}$  is small (about  $10^{-3}$  s),  $K_I T_{\Sigma i}$  is set to 0.5 so that  $K_I$  ranges from  $10^2$  to  $10^3 \text{ s}^{-1}$ ,  $\mu$  is about  $0.1 \text{ kg m}^2 \text{ s}^{-1}$ , and  $J$  has an immense value for large telescopes (about  $1.8 \times 10^4 \text{ kg m}^2$  in our system). As a result, on the Bode diagram, the break frequency  $\omega_1 = \mu/J$  is much smaller than another one  $\omega_2 = \sqrt{K_I/T_{\Sigma i}}$ , as is the cut-off frequency of  $G(s)$ . Thus, by ignoring the two-order term in Equation (5), the transfer function Equation (7) is approximated as

$$G(s) \approx \frac{k_m K_I}{(Js + \mu)(s + K_I)} = \frac{k_m K_I / J}{s^2 + (K_I + \mu/J)s + \mu K_I / J}. \tag{8}$$

Since this is a second-order linear model, the parameters can be identified by LS estimation via their discrete form and the sampled data of the measured system response (Keesman 2011). Using this approach, the result for this model is

$$G(s) = \frac{\Omega(s)}{I_q^*(s)} = \frac{0.08253}{s^2 + 0.3268s + 0.1594}, \tag{9}$$

where the unit of the input reference current  $i_q^*(t)$  is ampere, and the unit of the angular speed  $\omega(t)$  is scaled from  $\text{rad s}^{-1}$  to  $\text{deg s}^{-1}$ . Figure 3 illustrates one trial of the measured system response to the mixed sinusoidal input  $i_q^*(t) = 8 + 0.5 \sin(2\pi \cdot 0.1t) + 0.5 \sin(2\pi \cdot 0.05t) + 0.5 \sin(2\pi \cdot 0.02t)$  A,  $0 \leq t \leq 800$  s, compared to the model's response.

### 3 DESIGN OF THE H<sub>∞</sub> CONTROLLER

The design of a standard H<sub>∞</sub> controller consists of an electronic implementation of the transfer function matrix  $P(s)$  and the controller  $K(s)$ , as shown in Figure 4(a), forming a closed-loop linear system where  $w$  denotes the exogenous input (including the reference control and disturbances),  $u$

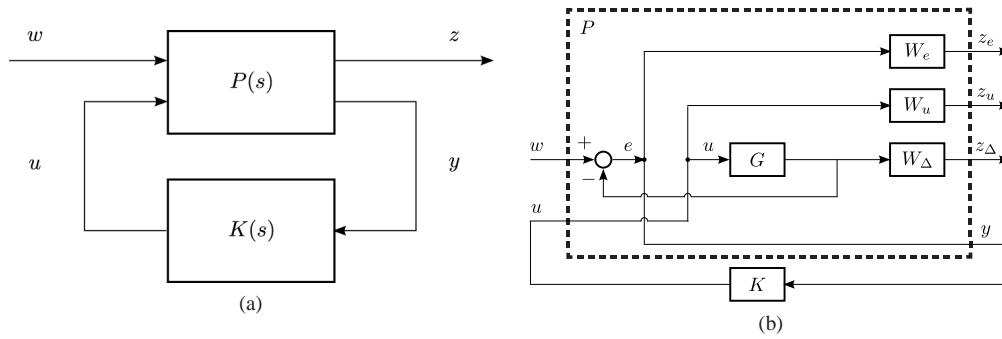


**Fig. 4** Standard  $H_\infty$  frame: (a)  $H_\infty$  control loop; (b) schematic diagram of the implementation of the 4-meter azimuth system with weighting functions.  $P(s)$  is an implementation of the augmented matrix for the linear system;  $K(s)$  is the  $H_\infty$  controller;  $w$  is the exogenous input (including the reference control and disturbances);  $z$  is the augmented output;  $u$  is the control signal;  $y$  is the measured output;  $G$  is the nominal transfer function of the control object;  $W_e$ ,  $W_u$ , and  $W_\Delta$  are the weighting functions of the tracking performance  $Z_e$ , the control input  $Z_u$ , and the robust performance  $Z_\Delta$  respectively.

denotes the control signal,  $y$  denotes the measured output, and  $z$  denotes the generalized performance formulated by actual requirements, e.g. the tracking performance. The relationships among the variables are described by

$$\begin{bmatrix} Z(s) \\ Y(s) \end{bmatrix} = \underbrace{\begin{bmatrix} P_{11}(s) & P_{12}(s) \\ P_{21}(s) & P_{22}(s) \end{bmatrix}}_{P(s)} \begin{bmatrix} W(s) \\ U(s) \end{bmatrix}, \quad (10)$$

$$U(s) = K(s)Y(s). \quad (11)$$

The objective is to produce a controller  $K(s)$  that first guarantees the stability of the closed-loop system and then minimizes the  $H_\infty$  norm of the system from  $w$  to  $z$ , i.e.

$$J = \inf_{K(s) \in S_k} \|T_{zw}(s)\|_\infty, \quad (12)$$

where  $S_k$  denotes the set of all the stabilizing controllers and

$$T_{zw}(s) = \frac{Z(s)}{W(s)} = P_{11}(s) + P_{12}(s)K(s) [I - P_{22}(s)K(s)]^{-1} P_{21}(s). \quad (13)$$

The solution to this optimization problem can be solved by the Algebraic Riccati Equations (Zhou et al. 1996).

The 4-meter azimuth closed-loop control problem for the 4-meter azimuth can be solved in the standard  $H_\infty$  frame with appropriate weighting functions, as shown in Figure 4(b). The weighting functions perform an important role in adjusting the sensitivity area and the uncertain boundary, averting the actuator from saturation, removing noise from the input, and suppressing a disturbance based on its design characteristics (Shen 1996). Under this frame, the behavior of the implementation of our system can be modeled by the augmented matrix

$$P(s) = \left[ \begin{array}{c|c} W_e & -W_e G \\ \hline 0 & W_u \\ 0 & W_\Delta G \\ \hline I & -G \end{array} \right], \quad (14)$$

where  $W_e(s)$ ,  $W_u(s)$  and  $W_\Delta(s)$  are the weighting functions of the tracking performance  $Z_e$ , the control input  $Z_u$ , and the robust performance  $Z_\Delta$ , respectively (Bibel & Malyevac 1992).

Although the design of weighting functions inevitably introduces a subjective tuning process, several guidelines can be followed (Ortega & Rubio 2004; Bibel & Malyevac 1992). To avoid saturation of the actuator, the reference current should be constrained by a constant less than the maximal feasible value  $I_{\max}$ , thus  $W_u(s)$  could be defined as a small constant close to  $1/I_{\max}$  (Bibel & Malyevac 1992). To adjust the tracking performance and the frequency response characteristic,  $W_e(s)$  adopts a low-pass filter structure (Kwakernaak 1993). To deal with uncertain factors and ensure robust, stable performance,  $|W_\Delta(j\omega)|$  can be designed to cover  $|1 - G(j\omega)/G_0(j\omega)|$  on the Bode diagram where  $G_0$  denotes the nominal transfer function of  $G$  (Mei et al. 2003). Because high disturbance rejection and high stability are required for this system, an equilibrium should be approached between the selections of  $W_e(s)$  and  $W_\Delta(s)$ . After a tuning process is applied, the weighting functions are defined as follows

$$W_u(s) = 0.05, \quad (15)$$

$$W_e(s) = \frac{3.5}{s^2 + 11s + 0.01}, \quad (16)$$

$$W_\Delta(s) = \frac{4.5s + 1}{s + 20}. \quad (17)$$

By solving the optimization problem defined by Equation (12) and compensating the controller gain, the H<sub>∞</sub> controller  $K(s)$  can be obtained as a fifth-order transfer function

$$K(s) = \frac{I_q^*(s)}{\Delta\Omega(s)} = \frac{9.1111(s + 11)(s + 20)(s^2 + 0.3268s + 0.1594)}{(s + 20)(s + 11)(s + 0.0009092)(s^2 + 1.874s + 1.69)} \quad (18)$$

$$= \frac{9.1111(s^2 + 0.3268s + 0.1594)}{(s + 0.0009092)(s^2 + 1.874s + 1.69)} \quad (19)$$

which can be simplified to third-order by canceling two pole-zero pairs  $z_1 = p_1 = -11$  and  $z_2 = p_2 = -20$ . The Bode diagrams of the weighting functions are shown in Figure 5(a). The Bode diagrams of Equations (18) and (19) are shown in Figure 5(b), which illustrates that the controller can keep almost the same frequency response after approximation—this feature benefits a simple realization of the controller. Using the controller defined by Equation (19), the behavior of the closed-loop system is described by

$$G_H(s) = \frac{\Omega(s)}{\Omega^*(s)} = \frac{K(s)G(s)}{1 + K(s)G(s)} = \frac{0.7519}{s^3 + 1.8749s^2 + 1.697s + 0.7534}, \quad (20)$$

where  $\Omega^*(s)$  is the reference angular velocity and  $G(s)$  is defined in Equation (9).

## 4 SIMULATIONS

### 4.1 Hypotheses Related to Model Inputs

To compare the performance between the H<sub>∞</sub> and the classic PI controller, the following idealizations are considered in the simulation:

- (1) All exogenous noises are equivalent to a disturbance  $\Delta\Omega^*$  affecting the reference  $\Omega^*$  in Equation (20). This results from the fact that many original disturbances can be traced in the models, thus their overall effect can be modeled as a properly chosen  $\Delta\Omega^*$ .

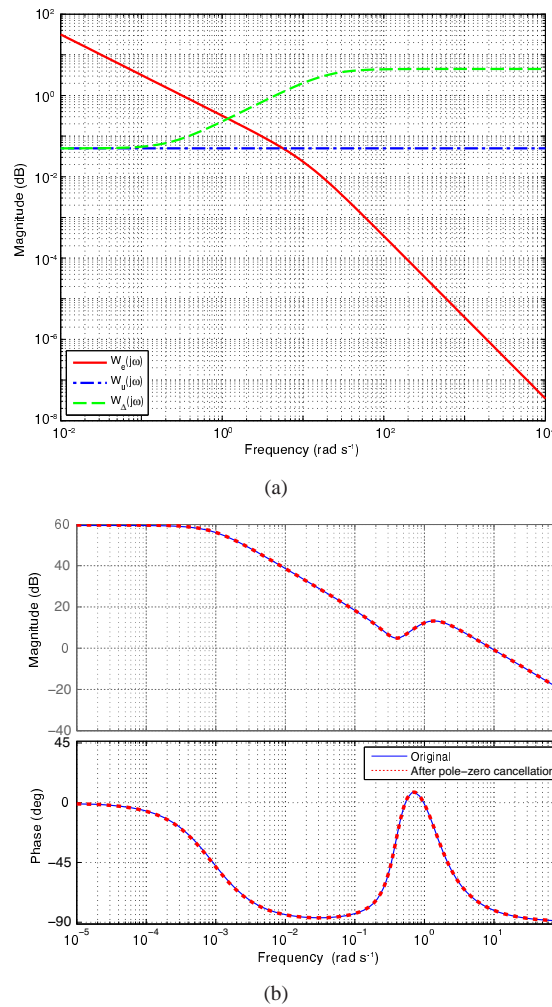


**Fig. 5** (a) Bode diagrams for the weighting functions  $W_e(s)$ ,  $W_u(s)$  and  $W_\Delta(s)$ . (b) Bode diagrams for transfer function of the original  $H_\infty$  controller  $K(s)$  Eq. (18) and the one after pole-zero cancellation Eq. (19). The superposed curves on the diagram show that Eq. (18) and Eq. (19) have almost the same frequency response.

- (2) Four cases of the input  $u(t)$ , i.e. the input function on the time domain, are examined in the simulation:  $u_0(t) = h(t)$  for a standard step response test,  $u_1(t) = \omega^* + w_1(t) = h(t) + a \sin 2\pi f_0 t$  for band-limited disturbances,  $u_2(t) = \omega^* + w_2(t) = h(t) + a \cdot \sum_{n=0}^{\infty} \delta(t - n/f_0)$  for periodic shocks, and  $u_3(t) = \omega^* + w_3(t) = \varepsilon(t)$  for random disturbances, where  $h(t)$  denotes the unit step function,  $a$  is a coefficient for tuning magnitude,  $f_0$  is a constant frequency (Hz),  $\delta(\cdot)$  denotes the Dirac delta function, and  $\varepsilon(t) \sim GP(1, \sigma)$  denotes a Gaussian process with mean 1 and standard deviation  $\sigma$ .

The  $u_1$  and  $u_2$  cases can roughly reflect the system response characteristics to different kinds of “colored” disturbances, and the  $u_3$  case represents the synthetic effect of all disturbances which can be considered random occurrences.

## 4.2 Simulation Results

Because a trade-off should be made in the choice of the controller gain, for the purpose of comparing two PI controllers  $K_{\text{PI}}(s) = k_p + k_i/s$  after tuning

$$K_{\text{PI}}(s) = 12.5 + \frac{0.8334}{s}, \quad (21)$$

$$K'_{\text{PI}}(s) = 9.2 + \frac{0.8474}{s}. \quad (22)$$

These are considered such that the larger  $k_p$  is, the less settling time is needed but the worse the disturbance suppression performs and *vice versa*. They will substitute for the H<sub>∞</sub> controller  $K(s)$  in Figure 4(b) in simulations. The transfer functions of the closed-loop system using the PI controllers whose behaviors are defined by Equation (21) and Equation (22) are respectively

$$G_{\text{PI}}(s) = \frac{K_{\text{PI}}(s)G(s)}{1 + K_{\text{PI}}(s)G(s)} = \frac{1.036s + 0.0688}{s^3 + 0.3268s^2 + 1.191s + 0.0688}, \quad (23)$$

$$G'_{\text{PI}}(s) = \frac{K'_{\text{PI}}(s)G(s)}{1 + K'_{\text{PI}}(s)G(s)} = \frac{0.7593s + 0.0699}{s^3 + 0.3268s^2 + 0.9187s + 0.0699}. \quad (24)$$

Four kinds of inputs,  $u_0$ ,  $u_1$ ,  $u_2$  and  $u_3$  mentioned in Subsection 4.1, will be applied to the systems  $G_{\text{H}}$ ,  $G_{\text{PI}}$  and  $G'_{\text{PI}}$  for the simulations.

The tests of  $u_1$  and  $u_2$  include five different disturbance frequencies  $f_0$ , 0.2, 0.5, 1.0, 1.5 and 2.0 Hz, which are chosen in accordance with the power spectral density analysis for the significant disturbances. The low frequency 0.2 Hz represents the disturbance caused by the stiffness deficiency of the rotator-axis and the hydraulic vibration, and the tests stop at 2.0 Hz because it is the Nyquist frequency of sampling. The test of  $u_3$  also adopts values of the standard deviation  $\sigma$  to be 0.2, 0.5, 1.0, 1.5, and 2.0. The closed-loop system responses in the tests of  $u_0$ ,  $u_1$ ,  $u_2$  and  $u_3$ , with cases 0.2, 0.5, 1.0 Hz for  $f_0$  and 0.2, 0.5, 1.0 for  $\sigma$ , are shown in Figure 6.

To quantify the *tracking error* and the *disturbance sensitivity* in the steady state, the response data  $y_i$ ,  $i = 1, 2, \dots, L$ , after the settling time are utilized to respectively define these two indicators

$$e_t = \sqrt{\frac{\sum_{k=1}^L (y_i - r)^2}{L}}, \quad (25)$$

$$e_s = \sqrt{\frac{\sum_{k=1}^L (y_i - \bar{y})^2}{L}}, \quad (26)$$

where  $r \equiv 1$  is the expected steady-state value for the unit step input, thus  $e_t$  measures the steady-state tracking error;  $\bar{y}$  denotes the average of all  $y_i$ , thus  $e_s$  measures the extent of steady-state oscillations, i.e. the disturbance sensitivity. The comparison of the indicators  $e_t$  and  $e_s$  for the controllers with inputs  $u_1(t)$ ,  $u_2(t)$  and  $u_3(t)$  is shown in Table 1. Results indicate that the H<sub>∞</sub> controller  $G_{\text{H}}(s)$  has a better steady-state performance, i.e. lower tracking error and disturbance sensitivity, than the PI controllers  $G_{\text{PI}}$  and  $G'_{\text{PI}}$ —on the working frequency band, the proposed H<sub>∞</sub> controller can:

- reduce the tracking error of the PI controllers on average by 68.8% for the sinusoidal disturbance, by 14.1% for the periodic impulse disturbance, and by 57.8% for the Gaussian disturbance;
- reduce the disturbance sensitivity of the PI controllers on average by 90.1% for the sinusoidal disturbance, by 91.3% for the periodic impulse disturbance, and by 58.32% for the Gaussian disturbance.

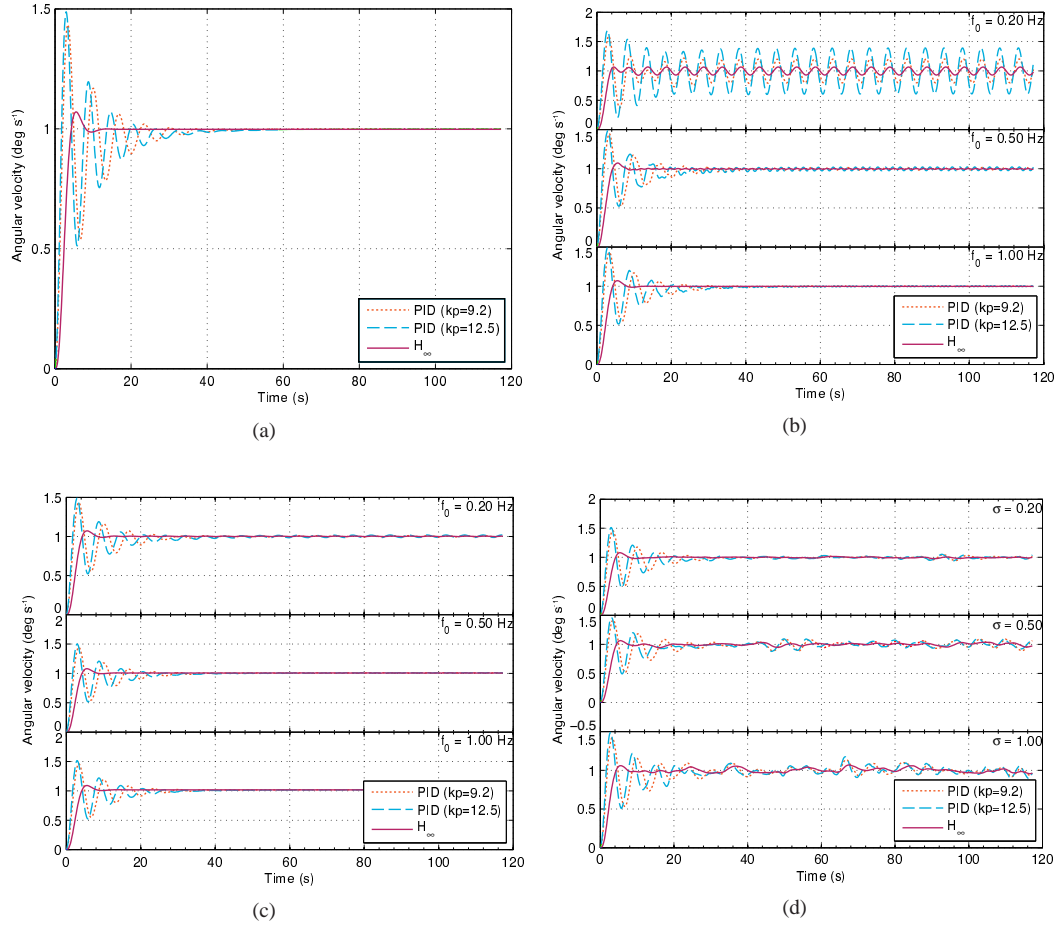


**Fig. 6** Closed-loop system responses to (a)  $u_0(t) = 1$ , (b)  $u_1(t) = 1 + 0.2 \sin 2\pi f_0 t$ , (c)  $u_2(t) = 1 + 0.2 \cdot \sum_{n=0}^{\infty} \delta(t - n/f_0)$ , and (d)  $u_3(t) \sim GP(1, \sigma)$ ,  $0 \leq t \leq 117.36$  s, where  $\delta(\cdot)$  denotes the Dirac delta function, and  $GP(1, \sigma)$  denotes the Gaussian process with mean 1 and standard deviation  $\sigma$ . The simulation results show that, in the sense of steady-state performance, the  $H_\infty$  controller  $G_H$  is better than the PI controllers  $G_{PI}$  and  $G'_{PI}$ . A detailed quantified advantage of  $G_H$  is shown in Table 1.

## 5 EXPERIMENT

### 5.1 Implementation of Controllers

As shown in Figure 4(b), the input of the controller  $K(s)$  is the error  $\Delta\Omega(s)$  between the reference angular velocity and its true value, and the output is the reference current  $I_q^*(s)$  for the motor model  $G(s)$ . For the transfer function  $K(s) = I_q^*(s)/\Delta\Omega(s)$ , the time domain controller can be obtained by  $i_q^*(t) = \mathcal{L}^{-1}\{\Delta\Omega(s)K(s)\}$ . After approximation and discretization for implementing on a small

**Table 1** Simulation: Comparison of Performance for Different Controllers in  $G_{PI}$ ,  $G'_{PI}$  and  $G_H$ 

Parameter	Tracking Error $e_t$ ( $\times 10^{-2}$ deg s $^{-1}$ )								
	Input $u_1$			Input $u_2$			Input $u_3$		
	$G_{PI}$	$G'_{PI}$	$G_H$	$G_{PI}$	$G'_{PI}$	$G_H$	$G_{PI}$	$G'_{PI}$	$G_H$
0.2	27.6	14.3	4.82	1.14	0.68	0.27	2.09	1.88	0.96
0.5	1.73	1.22	0.40	0.79	0.88	0.77	4.97	4.73	1.89
1.0	0.61	0.39	0.21	1.69	1.83	1.75	6.85	4.80	2.61
1.5	0.50	0.30	0.20	2.65	2.80	2.72	8.79	6.26	3.70
2.0	0.49	0.29	0.20	3.62	3.77	3.70	8.31	9.58	3.90

Parameter	Disturbance Sensitivity $e_s$ ( $\times 10^{-3}$ deg s $^{-1}$ )								
	Input $u_1$			Input $u_2$			Input $u_3$		
	$G_{PI}$	$G'_{PI}$	$G_H$	$G_{PI}$	$G'_{PI}$	$G_H$	$G_{PI}$	$G'_{PI}$	$G_H$
0.2	276	143	48.1	11.3	6.28	1.90	20.7	18.7	9.42
0.5	17.0	12.1	3.38	4.14	2.68	0.36	49.3	47.2	18.1
1.0	5.24	3.62	0.42	3.91	2.51	0.20	68.5	46.8	26.0
1.5	4.00	2.67	0.12	3.89	2.56	0.20	87.9	62.6	37.0
2.0	3.77	2.48	0.05	4.12	2.61	0.32	82.6	95.5	38.1

Notes: (1) The header ‘‘Parameter’’ denotes  $f_0$  for  $u_1(t)$  and  $u_2(t)$ , and  $\sigma$  for  $u_3(t)$ . (2)  $u_1(t) = 1 + 0.2 \sin 2\pi f_0 t$ ,  $u_2(t) = 1 + 0.2 \cdot \sum_{n=0}^{\infty} \delta(t - n/f_0)$ , and  $u_3(t) \sim GP(1, \sigma)$ . (3)  $e_t$  and  $e_s$  are defined in Equation (25) and Equation (26) respectively.

computer, the H<sub>∞</sub> controller Equation (19) is derived as

$$i_H(k) = \mathcal{L}^{-1} \{ \Delta\Omega(s)K(s) \} \quad (27)$$

$$\approx 9.11 \cdot \sum_{i=p}^k \Delta\omega(iT) \left\{ 0.0943 + 1.19e^{-0.937(k-i)T} \cos [0.901(k-i)T + 0.708] \right\} + c_1(\omega^*), \quad (28)$$

where  $k$  denotes the  $k$ -th timestep,  $k \in \mathbb{Z}^+$ ;  $T$  is the sampling interval (0.5 s in this experiment);  $p = 0$  is the theoretical solution but  $p = k - 19$  when  $k > 19$  is employed, because in practice the previous timesteps have little effect on  $i_H(k)$ ;  $c_1$  is an empirical constant, which is related to the reference angular velocity  $\omega^*$ , for approximating the initial values of the inverse Laplace transform result. The tuning process of  $c_1$  starts with the value that refers to the current-velocity open-loop relation for each specific angular velocity  $\omega^*$ , and stops when a satisfactory performance is achieved. In our experiment, the values of  $c_1$  are respectively 5.65, 5.75, 6.2, 6.45, 6.65, 7.12, 7.39, 7.42, and 7.78 A for 1, 1.5, 2, 2.5, 3, 3.5, 4, 4.5, and 5 deg s $^{-1}$  of  $\omega^*$ .

For comparison, a PI controller is properly tuned by using the simulation result as guidance. The PI controller used in the experiment is

$$K''_{PI}(s) = 12.5 + \frac{4.98 \times 10^{-5}}{s}. \quad (29)$$

Similarly, this controller is implemented as

$$i_{PI}(k) = \mathcal{L}^{-1} \{ \Delta\Omega(s)K''_{PI}(s) \} \quad (30)$$

$$= 12.5\Delta\omega(kT) + 4.98 \times 10^{-5} \cdot \sum_{i=0}^k \Delta\omega(iT) + c_2(\omega^*), \quad (31)$$

where  $c_2$  is also a value whose starting value is set to an empirical constant and whose tuning procedure is the same as  $c_1$ . The values of  $c_2$  in our experiment are respectively 5.65, 5.75, 6.2, 6.45, 7.6, 7.8, 7.12, 7.39, and 7.42 A for 1, 1.5, 2, 2.5, 3, 3.5, 4, 4.5, and 5 deg s $^{-1}$  of  $\omega^*$ .

**Table 2** Experiment: Performance Comparison of Controllers  $i_H(k)$  and  $i_{PI}(k)$ 

$\omega^*$ (deg s <sup>-1</sup> )	Tracking Error $e_t$			Disturbance Sensitivity $e_s$		
	$i_H$ (deg s <sup>-1</sup> )	$i_{PI}$ (deg s <sup>-1</sup> )	Improved (%)	$i_H$ (deg s <sup>-1</sup> )	$i_{PI}$ (deg s <sup>-1</sup> )	Improved (%)
1.0	0.0139	0.0232	40.09	0.0126	0.0222	43.40
1.5	0.0179	0.0338	47.04	0.0143	0.0210	31.78
2.0	0.0135	0.0601	77.54	0.0129	0.0283	54.47
2.5	0.0146	0.0315	64.99	0.0144	0.0416	65.44
3.0	0.0090	0.0443	79.68	0.0090	0.0389	76.91
3.5	0.0241	0.0348	30.75	0.0220	0.0275	20.00
4.0	0.0216	0.0421	48.69	0.0196	0.0417	53.02
4.5	0.0193	0.0392	50.77	0.0191	0.0278	31.32
5.0	0.0186	0.0963	80.69	0.0169	0.0957	82.30

Notes: (1)  $i_H(k)$  is the  $H_\infty$  controller defined in Equation (28) and  $i_{PI}(k)$  is the PI controller defined in Equation (31). (2)  $\omega^*$  is the reference angular velocity input for the closed-loop system. (3)  $e_t$  and  $e_s$  are defined in Equation (25) and Equation (26) respectively. (4) The “Improved” indicator for Tracking Error  $e_t$  is calculated by  $(e_t\{i_{PI}\} - e_t\{i_H\})/e_t\{i_{PI}\} \times 100\%$  and the “Improved” indicator for Disturbance Sensitivity  $e_s$  is calculated by  $(e_s\{i_{PI}\} - e_s\{i_H\})/e_s\{i_{PI}\} \times 100\%$ .

Finally, an upper bound for both  $i_H(k)$  and  $i_{PI}(k)$  should be assigned according to engineering limits on the system and safety considerations. Pragmatic values of the upper bound used in our experiment are 0–17.68 A under angular velocities 1–5 deg s<sup>-1</sup>. Any calculated  $i_H(k)$  or  $i_{PI}(k)$  that exceeds the upper bound will be restricted to the feasible region.

## 5.2 Experimental Results

Nine reference angular velocities  $\omega^*$  are implemented as inputs to the closed-loop system: 1.0, 1.5, 2.0, 2.5, 3.0, 3.5, 4.0, 4.5 and 5.0 deg s<sup>-1</sup>. The outputs of the closed-loop system, which are real angular velocities measured by the photoelectric encoder, are illustrated in Figure 7: (a) for the system using the  $H_\infty$  controller  $i_H(k)$  described in Equation (28), and (b) for the system using the PI controller  $i_{PI}(k)$  described in Equation (31). Quantified results that can be used for comparison of the tracking error  $e_t$  and the disturbance sensitivity  $e_s$  are shown in Table 2. Results indicate that the  $H_\infty$  controller has better behavior in terms of disturbance rejection and stability, and is able to significantly improve the steady-state performance of the PI controller for reducing the tracking error by 30.75%–80.68% (average 58%) and the disturbance sensitivity by 20.0%–82.3% (average 51%).

## 6 CONCLUSIONS

This paper reviews the external disturbances that exist in several well-known large aperture telescopes such as VLT, GTC and TMT, and briefly analyzes insufficiency in their control strategies that are mainly carried out with the PID controller. Based on the necessities of disturbance rejection and stabilization for such kind of telescopes, we establish an  $H_\infty$  controller and highlight its advantages on an experimental 4-meter azimuth direct-drive control system step by step. First, the model of the real system is identified by the LS method. Second, an  $H_\infty$  controller is designed and then compared with two tuned PI controllers in the simulations, which include three different contaminated step signals. Finally, guided by the simulation results, an  $H_\infty$  controller and a tuned PI controller, used as a comparison, are implemented in a real velocity closed-loop control system. The experimental results show that the  $H_\infty$  controller can improve the performance in terms of disturbance rejection and stabilization with the corresponding quantitative indicators.

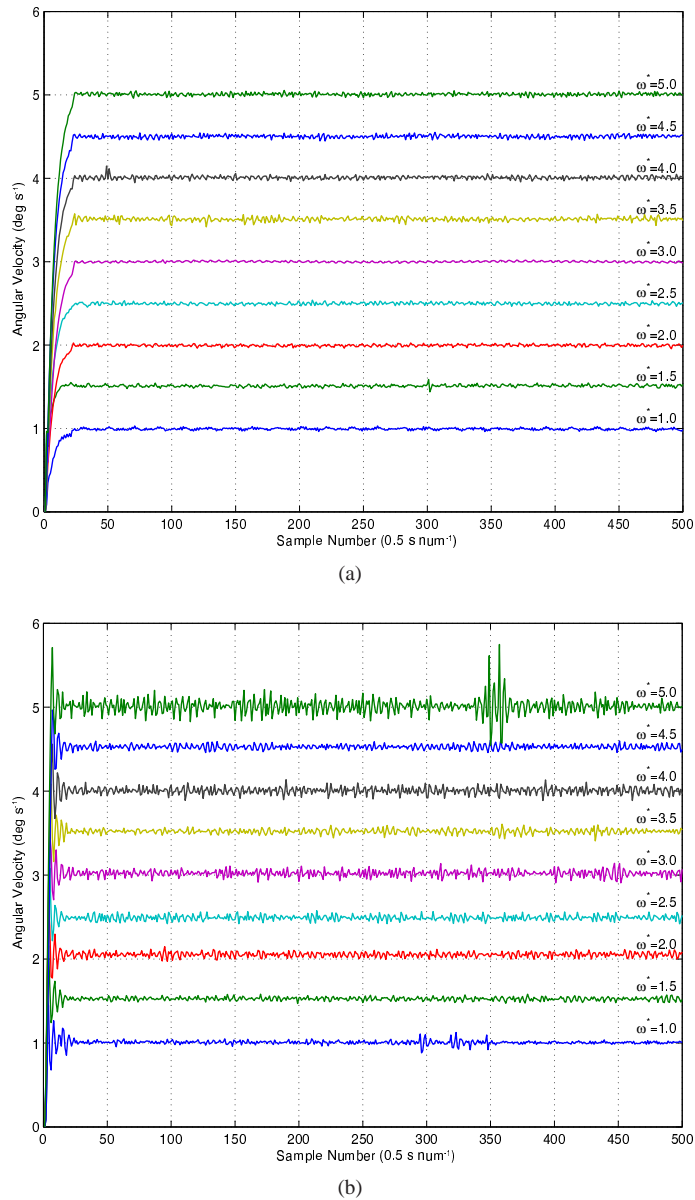


**Fig. 7** Real angular velocities of the closed-loop system that are responses to the reference inputs  $\omega^*$  from 1.0 to 5.0 deg s<sup>-1</sup>, controlled by (a) the H<sub>∞</sub> controller  $i_H(k)$  described in Eq. (28), and (b) the PI controller  $i_{PI}(k)$  described in Eq. (31).

**Acknowledgements** This work is supported by the Knowledge Innovation Program of the Chinese Academy of Sciences (No. KJXC2-YW-T17) under the leadership of Academician Xiangqun Cui, and supported by the National Natural Science Foundation of China (No. 11373052) We also appreciate Prof. Kanjian Zhang from Southeast University (China) for the discussion with us on H<sub>∞</sub> control issues.

## References

- Angeli, G. Z., Cho, M. K., Sheehan, M., & Stepp, L. M. 2002, in *Workshop on Integrated Modeling of Telescopes*, 72–83 (International Society for Optics and Photonics)
- Antoniou, I., Asimakopoulos, D., Fragoulis, A., et al. 1992, *Journal of Wind Engineering and Industrial Aerodynamics*, 39, 343
- Baris Ulutas, D. K., & Jennifer Dunn, E. J. P., Afzal Suleman 2012, *Mechatronics*, 22, 121
- Bibel, J. E., & Malyevac, D. S. 1992, *Guidelines for the Selection of Weighting Functions for H-infinity Control*, Tech. rep., DTIC Document
- Carlstrom, J. E., Ade, P. A. R., Aird, K. A., et al. 2011, *PASP*, 123, 568
- Cho, M. K., Stepp, L. M., & Kim, S. 2001, in *International Symposium on Optical Science and Technology*, 302 (International Society for Optics and Photonics)
- Dixon, J., Tepper, S., & Morán, L. 1996, *IEEE Proceedings-Electric Power Applications*, 143, 301
- Dorf, R. C., & Bishop, R. H. 2011, *Modern Control Systems* (Pearson)
- Erm, T., & Gutierrez, P. 2000, in *Astronomical Telescopes and Instrumentation*, 490 (International Society for Optics and Photonics)
- Farahani, A., Kolesnikov, A., Cochran, L., Hull, C., & Johns, M. 2012, in *SPIE Astronomical Telescopes+ Instrumentation*, 84440U (International Society for Optics and Photonics)
- Gawronski, W. 2001, *IEEE Antennas and Propagation Magazine*, 43, 52
- Keesman, K. J. 2011, *System Identification: an Introduction* (Springer)
- Krause, P. C., Wasynczuk, O., Sudhoff, S. D., & Pekarek, S. 2013, *Analysis of Electric Machinery and Drive Systems*, 75 (John Wiley & Sons)
- Kwakernaak, H. 1993, *Automatica*, 29, 255
- Louis, J.-P. 2013, *Control of Synchronous Motors* (John Wiley & Sons)
- Mei, S. W., Shen, T.-L., & Liu, K. Z. 2003, *M. Tsinghua University Publication*, 94
- Ortega, M., & Rubio, F. 2004, *Journal of Process Control*, 14, 89
- Ravensbergen, M. 1994, in *1994 Symposium on Astronomical Telescopes & Instrumentation for the 21st Century*, 997 (International Society for Optics and Photonics)
- Ruan, Y., & Chen, W. 2006, *Motion Control Systems* (Beijing: Tsinghua Univ. Press)
- Shen, T. 1996, *H<sub>∞</sub> Control Theory and Application* (Beijing: Tsinghua Univ. Press)
- Suárez, M., Rosich, J., Ortega, J., & Pazos, A. 2008, in *SPIE Astronomical Telescopes+ Instrumentation*, 70190J (International Society for Optics and Photonics)
- Zhou, K., Doyle, J. C., Glover, K., et al. 1996, *Robust and Optimal Control*, 40 (New Jersey: Prentice Hall)